Hindawi Publishing Corporation
Journal of Nanomaterials
Volume 2014, Article ID 723057, 9 pages
http://dx.doi.org/10.1155/2014/723057

Research Article

Preparation Method of Co_3O_4 Nanoparticles Using Degreasing Cotton and Their Electrochemical Performances in Supercapacitors

Hongyan Xu,[1] Libo Gao,[2] Qiang Zhang,[2] Junyang Li,[2] Jiangtao Diwu,[1] Xiujian Chou,[2] Jun Tang,[2] and Chenyang Xue[2]

[1] *School of Materials Science and Engineering, North University of China, No. 3 Xueyuan Road, Taiyuan, Shanxi 030051, China*
[2] *Key Laboratory of Instrumentation Science and Dynamic Measurement of Ministry of Education, North University of China, No. 3 Xueyuan Road, Taiyuan, Shanxi 030051, China*

Correspondence should be addressed to Chenyang Xue; xuechenyang@nuc.edu.cn

Received 11 December 2013; Revised 18 February 2014; Accepted 19 February 2014; Published 20 March 2014

Academic Editor: Matthew T. Cole

Co_3O_4 nanoparticles were fabricated by a novel, facile, and environment-friendly carbon-assisted method using degreasing cotton. Structural and morphological characterizations were performed using X-ray diffraction (XRD), scanning electron microscopy (SEM), and transmission electron microscopy (TEM). The component of the sample obtained at different temperatures was measured by Fourier transform infrared spectroscopy (FTIR) and X-ray photoelectron spectroscopy (XPS). Nitrogen adsorption and desorption isotherms were utilized to reveal the specific surface areas. The formation mechanism of Co_3O_4 nanoparticles was also proposed, demonstrating that the additive degreasing cotton played an indispensable role in the process of synthesizing the sample. The resultant Co_3O_4 sample calcined at 600°C exhibited superior electrochemical performance with better specific capacitance and long-term cycling life, due to its high specific surface areas and pores structures. Additionally, it has been proved that this facile synthetic strategy can be extended to produce other metal oxide materials (e.g., Fe_3O_4). As a consequence, the carbon-assisted method using degreasing cotton accompanied a promising prospect for practical application.

1. Introduction

In recent years, supercapacitors have been intensively explored owing to their large energy density, fast recharge capability, and long-term cycling life. Hence, they are widely used in many areas, such as backup power source, hybrid electric vehicle, and digital communication devices [1–3]. As the core component of supercapacitors, electrode materials including carbon materials [4, 5], transition metal oxides [6, 7], and conducting polymers [8, 9] have a crucial effect on the performance of supercapacitors. The carbon materials are relatively low-cost and stable, but they exhibit poor specific capacitance, limiting their wide application. Similarly, the short cycle life of conducting polymers hinders their practical application. RuO_2 possess a higher specific capacitance than conventional materials. Nevertheless, the high cost of Ru restricts its commercial application. Therefore, it is essential to find other new materials with better performance and low-cost.

Co_3O_4 has gained recognition as one of the most ideal electrode material for supercapacitors due to its extremely high theoretical specific capacitance of 3,560 F/g. In addition, it is known to all that the crystallinity, morphology, specific surface area, chemical compositions, and structural stability of nanomaterials all have dramatic effects on the performance of the supercapacitors [10–12]. In this regard, much effort has been devoted to synthesizing Co_3O_4 with well-controlled dimensionality, sizes, and crystal structure. Ma et al. reported a carbon-assisted carbothermal method to synthesis the single-crystalline Co_3O_4 octahedral cages with tunable surface aperture. The prepared Co_3O_4 exhibits a high specific surface area and superior electrochemical performance due to its unique architecture [13]. Du et al. used the carbon spheres obtained through hydrothermal carbonization as the sacrificial template and successfully synthesized Co_3O_4 hollow spheres by a one-pot calcinations method [14]. Additionally, it was proved that the carbon spheres soft-template and the NH_3 released from hexamethylenetetramine played key roles in the formation of these novel structures. Liu et al. fabricated Co_3O_4 nanowire@MnO_2 ultrathin nanosheet core/shell arrays through a general 3D interfacial carbon-assisted hydrothermal method. And the array synthesized shows a high capacitance with good cycle performance and remarkable rate capability [15]. Zhang et al. described the synthesis of high purity octahedral Co_3O_4 with the help of carbon materials using one step microwave reaction [16]. On the basis of the above reports, the carbon-assisted route was deemed to one of the most practical techniques to fabricate well-controlled Co_3O_4 with high purity and outstanding properties on account of its simple synthetic process and affordable carbon materials. In particular, the carbon can provide a weak reduction environment, which was beneficial to promote nuclei oriented growth in the solid state reaction [17–22]. The downside of the method mentioned in these reports was, of course, that the carbon materials had to be synthesized through a series of routes before the preparation of Co_3O_4. What was worse, the byproducts (e.g., NH_3) produced may be unfriendly to the environment.

Herein, we report on the preparation of Co_3O_4 nanoparticles through a novel, facile, and environment-friendly carbon-assisted method using degreasing cotton. To the best of our knowledge, this is the first time that the degreasing cotton was used as the carbon material to prepare Co_3O_4. In our work, the Co_3O_4 nanospheres were successfully synthesized and the formation mechanism of Co_3O_4 was proposed. Their electrochemical capacitance behavior with high capacitance and durable cycle life in 6 M KOH solution was also discussed. Encouragingly, superparamagnetic Fe_3O_4 was also successfully fabricated via the same method as reported in our previous paper [23].

2. Materials and Methods

2.1. Synthesis. All chemicals were of analytical grade and used as received without further purification. In a typical experimental process, 17.46 g $Co(NO_3)_2{\cdot}6H_2O$ was dissolved in a 20 mL deionized water under agitated stirring for 10 min to get a pink solution. Then, 1.5 g degreasing cotton which was cut into pieces was immersed into the pink solution and kept in an ultrasonic bath for 10 min. Subsequently, the degreasing cotton was collected and transferred into a quartz petri dish. The whole reaction system was performed at 200, 400, and 600°C, respectively, for 2 h in air in the tube furnace (OTF-1200X-III, Hefei, China) with a heating rate of 10°C min^{-1}. Accordingly, the obtained samples with degreasing cotton were denoted as Co-200, Co-400, and Co-600, respectively.

2.2. Characterization. The crystal structure of the sample was studied by X-ray diffraction (XRD, a Bruker D8, λ = 1.5406 Å) in the 2θ of 10–80° with scan rate of 10°/min and Cu Kα radiation, 40 KV. Scanning electron microscopy (SEM) images were performed on a HitachiS-4800 scanning electron microscope. The particle shapes and sizes were characterized by TEM measurements (JEOL JEM-1200EX) with an accelerating voltage of 120 KV. Specific surface areas and pore size distributions were computed from the results of N_2 physisorption at 77 K (Micromeritics ASAP 2020) by using the BET (Brunauer-Emmett-Teller) and BJH (Barrett-Joyner-Halenda). Fourier transform infrared (FT-IR) spectra of samples were recorded from KBr pellets in the range of 500–4000 cm^{-1} on an Avatar 360 spectrometer.

2.3. Electrochemical Performance Measurements. All electrochemical measurements were performed by an electrochemical workstation (CHI660E, Shanghai, China) in a three-electrode cell system with Pt foil as the counter electrode and a standard calomel electrode (SCE) as the reference electrode at room temperature. The working electrode was prepared by mixing of the prepared Co_3O_4, acetylene black as the conducting agent, and polyvinylidene fluoride (PVDF) with a ratio of 8 : 1.5 : 0.5 in a few drops of N-Methyl-2-pyrrolidone. Subsequently, the mixture was pressed onto a treated nickel foam (10 mm × 5 mm × 1 mm, 110PPI, 300 g ± 20/m^2, Taiyuan Yingze Lzy Battery Sales Department, China) which served as a current collector under a pressure of 10 MPa and dried at 80°C for 12 h. The 0.5 cm^2 electrode contains 11 mg pure Co_3O_4 nanoparticles and the thickness of the electrode is estimated 0.237 mm by the Digital Indicators (Guilin Guanglu Measuring Instrument Co., Ltd., China). The electrolyte used was 6 M KOH solution. Cyclic voltammograms (CV) were conducted within the potential range from −0.1 to 0.50 V at various scan rates. The constant current charge-discharge measurement was carried out at a current density of 3 Ag^{-1} within a potential window from 0 to 0.50 V. The impedance spectra were estimated by applying an AC voltage of 5 mV amplitude in the frequency range from 0.01 Hz to 100 kHz.

3. Results and Discussion

3.1. The Structures and Morphologies of Samples. The phase identity of the samples calcined at different temperatures (200~600°C) was determined by X-ray diffraction. As shown in Figure 1, all the calcined products were in good agreement with the standard spinel cubic Co_3O_4 spectrum [PDF No. 42-1467]. Sample Co-200 should be a mixture of $CoCO_3$ and Co_3O_4, reflected by characteristic peaks of $CoCO_3$ [PDF No. 78-209] at 24.5, 42.4, and 54.0°, respectively. Besides, sample Co-600 showed strong and sharp shapes of peaks, and no impurity peaks were observed, manifesting the successful preparation of Co_3O_4. Furthermore, the peak intensity increased and peak width decreased with increasing calcination temperature, suggesting that higher temperature had a good favor to the crystallization of Co_3O_4. According to Scherrer's formula, $D = 0.89\lambda/(B\cos\theta)$ (D, average dimension of crystallites; λ, the X-ray wavelength; θ, the Bragg Angle; B, the pure diffraction broadening of a peak at half-height) the crystalline size of Co-200, Co-400, and Co-600, calculated from the strongest peak located at (311) plan were estimated to be 24.22, 29.77, and 51.64 nm, respectively. The increase of crystal size can be explained by the ripening

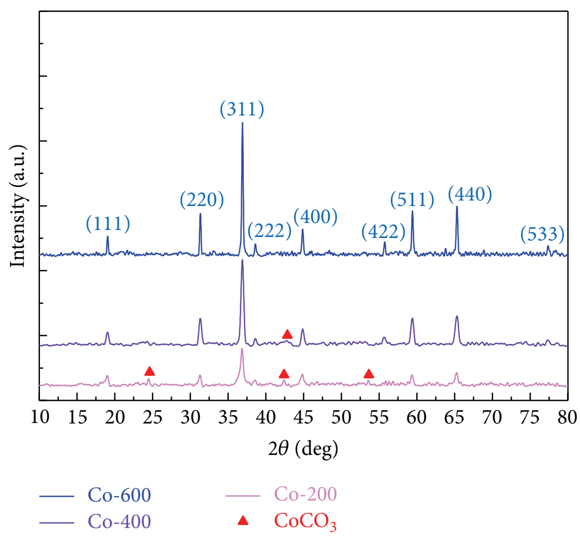

Figure 1: XRD patterns of different samples obtained at 200~600°C.

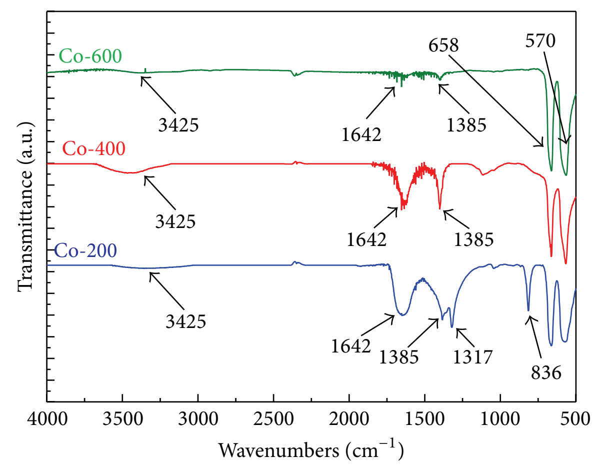

Figure 2: IR spectra of different samples obtained at 200~600°C.

and agglomeration of the small crystallite during calcination procedure at high temperature [24]. In conclusion, the results implied that the calcination temperature had a significant effect on the Co_3O_4.

To better understand the possible phase evolution, the FT-IR spectrum is depicted to reveal the composition of the product calcined at different temperatures. In Figure 2, the strong peaks at 3425 and 1642 cm^{-1} are attributed to the molecular water and hydrogen-bond O–H groups [25]. The bands around 836 and 1317 cm^{-1} are associated with the characteristic peaks of CO_3^{2-} anions and the stretching vibrations of band in C–O, respectively. The first band at 570 cm^{-1} is associated with the OB3 (where B represents Co^{3+} in an octahedral hole) vibration in the spinel lattice, while the second band at 658 cm^{-1} is attributed to the ABO3 vibration (where A denotes the Co^{2+} in a tetrahedral hole), confirming the existence of Co_3O_4 [26, 27]. The band at 1385 cm^{-1} which becomes weak with the increasing temperature suggests that NO_3^- anions exist as free anions with high *D3h* symmetry, and thus few of the NO_3^- anions are coordinated to Co^{2+} in the solid phase [28, 29]. This may be the reason why there is no spectrum detection of $Co(NO_3)_2$ in XRD spectrum, in Figure 1. The FTIR spectrum provides further evidence of the phase structure changes, which correspond with the XRD results.

Figure 3 shows the XPS measurement of sample Co-600, which is carried out for further investigation of the chemical composition. Figure 3(a) shows the regional Co 2p spectra of Co-600. Two strong peaks of Co $2p_{3/2}$ and Co $2p_{1/2}$ center at 780.4 and 795.6 eV, respectively. The positions of the peaks are similar to the results reported elsewhere [30, 31]. The energy difference between the peak of Co $2p_{3/2}$-Co $2p_{1/2}$ splitting is about 15 eV, suggesting the presence of Co^{2+} and Co^{3+} species in the sample. O 1s peak at 531 eV is found in Figure 3(b), which should be attributed to the lattice oxygen of Co_3O_4. The major peak of C 1s is observed in Figure 3(c), which can be assigned to the product calcined of degreasing cotton. The full survey scan spectrum is provided in Figure 3(d). All the above characteristics suggest that the sample Co-600 is pure Co_3O_4.

To observe the morphology and microstructure of the product calcined at different temperatures (200~600°C), SEM and TEM are employed in Figure 4. Figures 4(a) and 4(b) clearly imply that the sample calcined at 200°C is a mixture of sphere-like products in large size and nanoparticles with irregular shape. From Figure 4(c), it was apparent that the nanoparticles are in the period of nucleation, and the particles are seriously aggregated. Meanwhile, in Figure 4(d), the particles are sphere-like structures with an average size of 30 nm, which is very close to the particle size calculated by the Scherrer's formula according to the XRD pattern (Figure 1). In addition, disordered hole-like arrangement of pores is clearly seen from Figure 4(d), suggesting the formation of porous structure, which may be formed due to the agglomerated nanoparticles [14]. Surprisingly, it can be clearly seen from the panoramic view (Figures 4(e) and 4(f)) that the sample contains uniform and weak agglomerated Co_3O_4 nanospheres with 50 nm in diameter after calcinations at 600°C. The reason will be discussed below. Moreover, disordered hole-like arrangement of pores also can be seen in Figure 4(e).

Brunauer-Emmett-Teller (BET) surface areas and Barrett-Joyner-Halenda (BJH) pore size distributions of the as prepared Co-600 are shown in Figure 5. The isotherms exhibit the typical type of IV, according to the IUPAC classification. There is a sharp increase in the uptake of N_2 at higher relative pressure ($p/p_0 > 0.9$), suggesting the existence of macropores resulted from the interparticle space in the samples [32], which facilitates the electrolyte/ion accessibility to nanoparticles. Additionally, an obvious macropore region is observed which is due to the higher fraction of macropores. According to the corresponding BJH pore size distribution curve, the pore size distribution has a relatively intense peak of 10 nm and a wide distribution centered at 60 nm (>50 nm), showing a bimodal nature and hierarchical porosity composed of mesopores and macropores. The BET surface

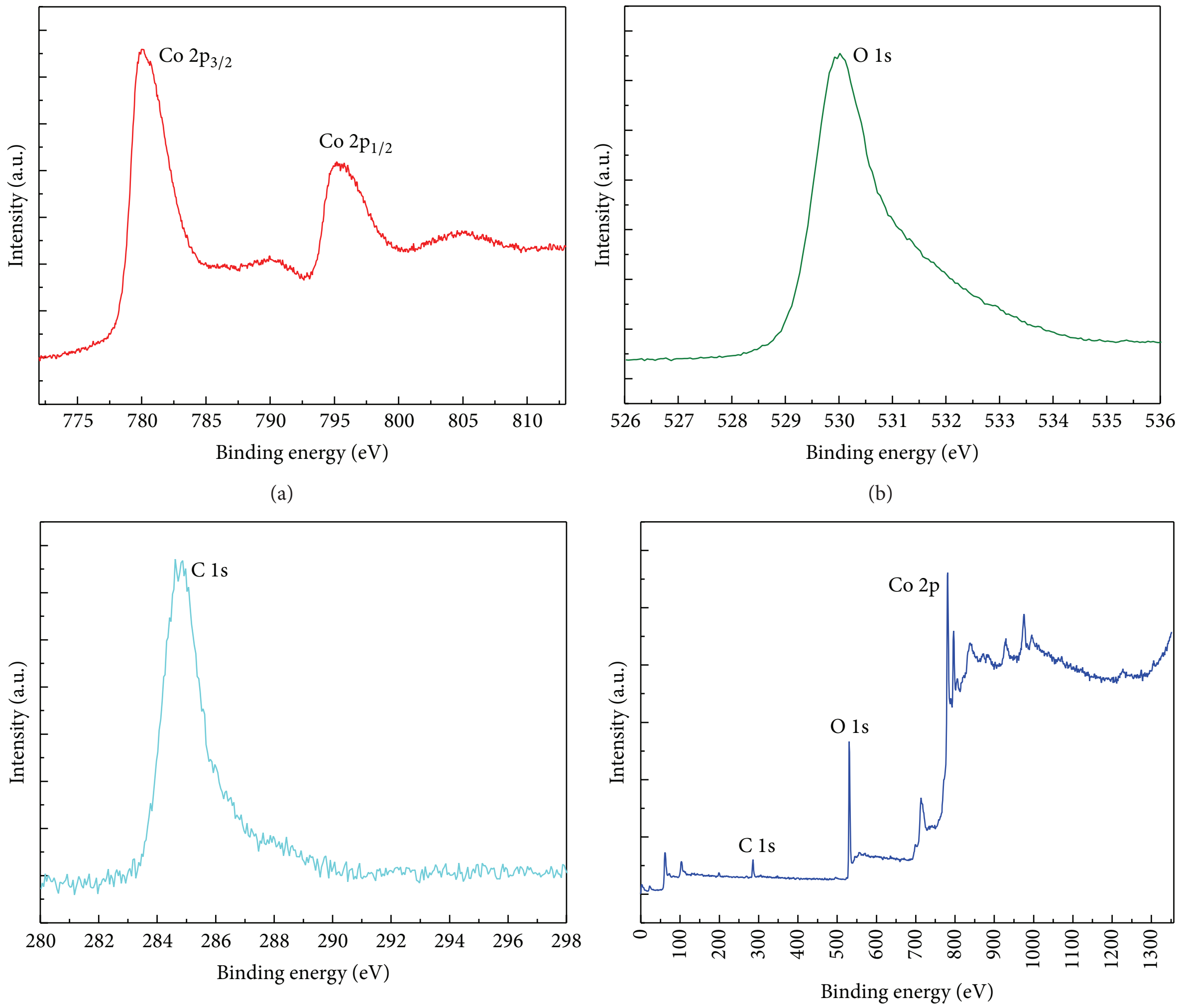

FIGURE 3: XPS spectra of the Co-600:(a) Co 2p spectra of Co-600, (b) O 1s spectra of Co-600, (c) C 1s spectra of Co-600, and (d) full survey scan spectrum of Co-600.

areas were calculated to be 17.64 m^2/g and the average pore size is 23.67 nm. Supposing that the Co_3O_4 nanoparticles are almost spherical (as confirmed by SEM and TEM), the surface area can be calculated as the equation $D_{BET} = 6000/(\rho * S_{BET})$ [26], where D_{BET} represents the diameter of a spherical particle (nm) and ρ and S_{BET} represent the theoretical density of Co_3O_4 (6.05 g/cm^3) and the specific surface area of Co_3O_4 (m^2/g), respectively. The results show that the particle size is 56.22 nm, which is very close to the XRD and TEM values. Generally, the carbon-assisted method using degreasing cotton provides a facile and environmental route for the preparation of the sample with both high BET surface area and high crystallization.

3.2. Formation Mechanism. Based on the analysis above, the formation and changing procedure of Co_3O_4 nanoparticles can be described as shown in Figure 6. It is revealed that the synthetic process includes two steps, the precursors gradually transform from $Co(NO_3)_2$ to $CoCO_3$ and finally to pure Co_3O_4, as the calcination temperature increased. Meanwhile, the $CoCO_3$ underwent both the phase and shape changed during calcinations. The morphology of sample changed from irregular shape to sphere-like to sphere and the similar results is observed in Wang et al.'s work [13]. Particularly noteworthy is that the degreasing cotton is indispensable in the successful formation of Co_3O_4. On the one hand, the carbon resulted from the thermal treatment of degreasing cotton plays an important role in the synthesis of Co_3O_4 nanospheres, because Wang et al. [13] and Wang [33] had proved that the recrystallization took place between Co_3O_4 and carbon during carbothermal reaction, this also may be the reason of the phenomenon observed in Figure 4. On the other hand, CO_2 has a crucial effect on the nucleation of $CoCO_3$. Furthermore, additive degreasing cotton is decomposed completely and released, leading to the formation of porous structure of Co_3O_4 [34]. Corresponding reactions are shown as follows:

$$(C_6H_{10}O_5)_n + 6nO_2 \longrightarrow 6nCO_2 + 5nH_2O \quad (1)$$

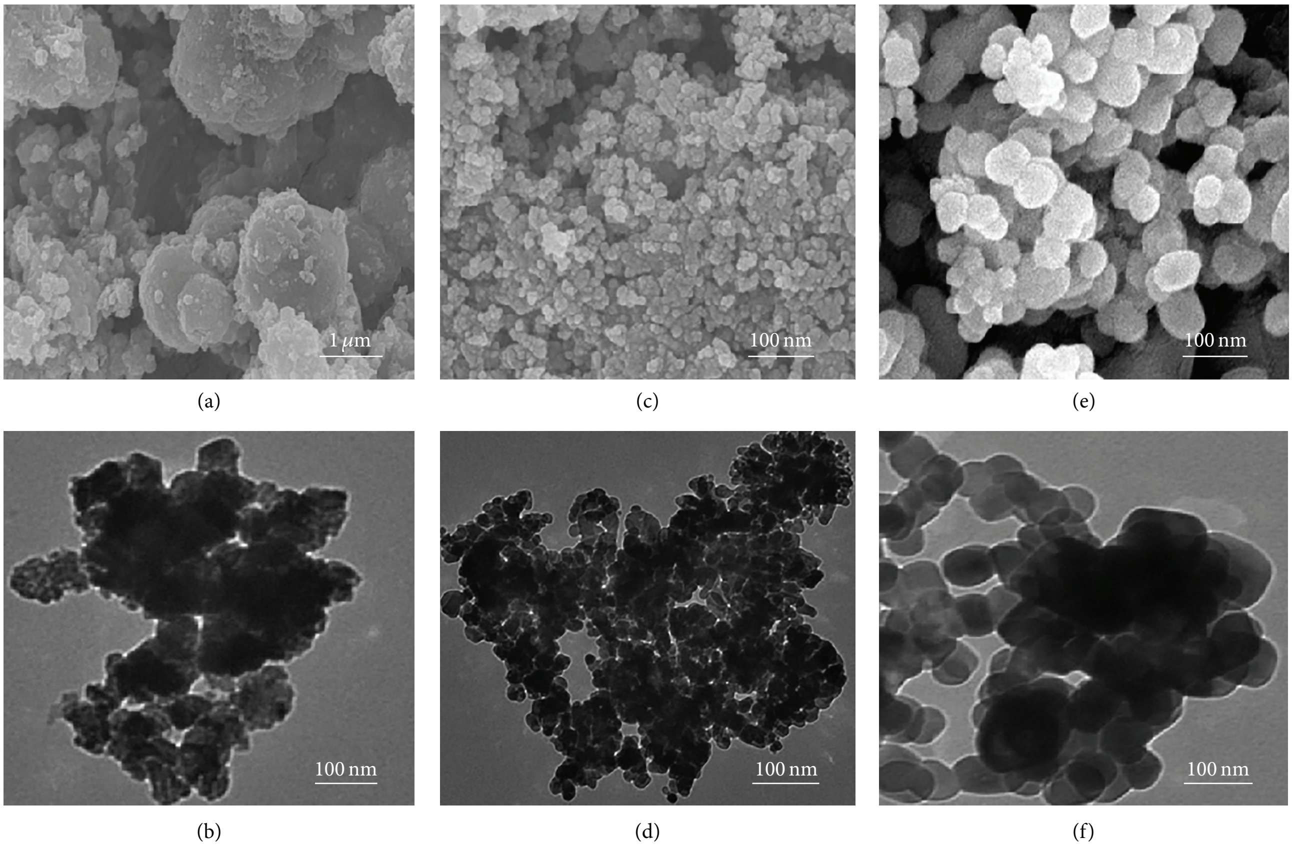

FIGURE 4: SEM and TEM images of samples obtained at different temperatures. (a) and (b) 200°C, (c) and (d) 400°C, and (e) and (f) 600°C.

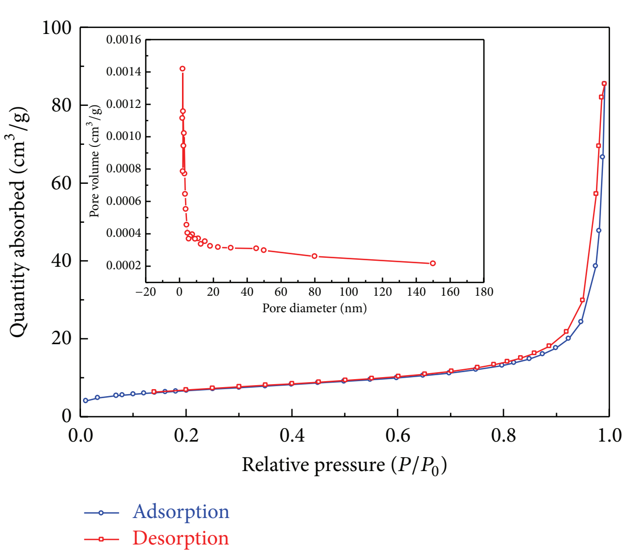

FIGURE 5: Nitrogen adsorption-desorption isotherms of Co-600 (the insert image is the BJH pore size distributions of Co-600).

$$CO_2 + H_2O \longrightarrow CO_3^{2-} + 2H^+ \quad (2)$$

$$Co^{2+} + CO_3^{2-} \longrightarrow CoCO_3 \quad (3)$$

$$3CoCO_3 + \frac{1}{2}O_2 \longrightarrow Co_3O_4 + 3CO_2 \quad (4)$$

However, considering the limitations in length, the more detailed information on the formation mechanism of Co_3O_4 will be discussed in our next stage of researches.

3.3. Electrochemical Performances. Figure 7(a) illustrates the potential versus time for the Co_3O_4 obtained by the annealing temperature of 200, 400, and 600°C at the scan rate of 10 mV/s. All curves exhibit apparent pseudocapacitance features with similar line-type, demonstrating the capacitance that mainly derives from the rapid reversible redox of active materials (Co_3O_4) within the potential range from −0.1 V to 0.5 V [35]. Additionally, compared with Co-200 and Co-400, Co-600 has the largest areas and the highest polarization voltage, suggesting that the Co-600 has the best specific capacitance (C) and the fastest diffusion of electrolytic ions for the electrochemical oxidation. Such behavior is probably due to the high crystallinity of Co-600 and interconnected macropores in Co-600 mentioned above. The two redox couples P_1/P_4 and P_2/P_3 stand for the following reactions [36]:

$$Co_3O_4 + OH^- + H_2O \longleftrightarrow 3CoOOH + e^- \quad (5)$$

$$CoOOH + OH^- \longleftrightarrow CoO_2 + H_2O + e^- \quad (6)$$

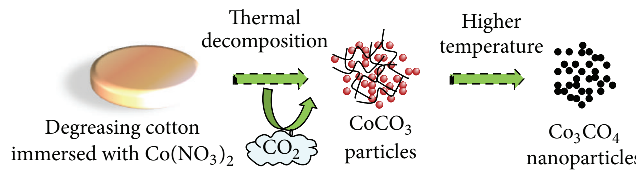

FIGURE 6: The formation and changing process of Co_3O_4 nanoparticles.

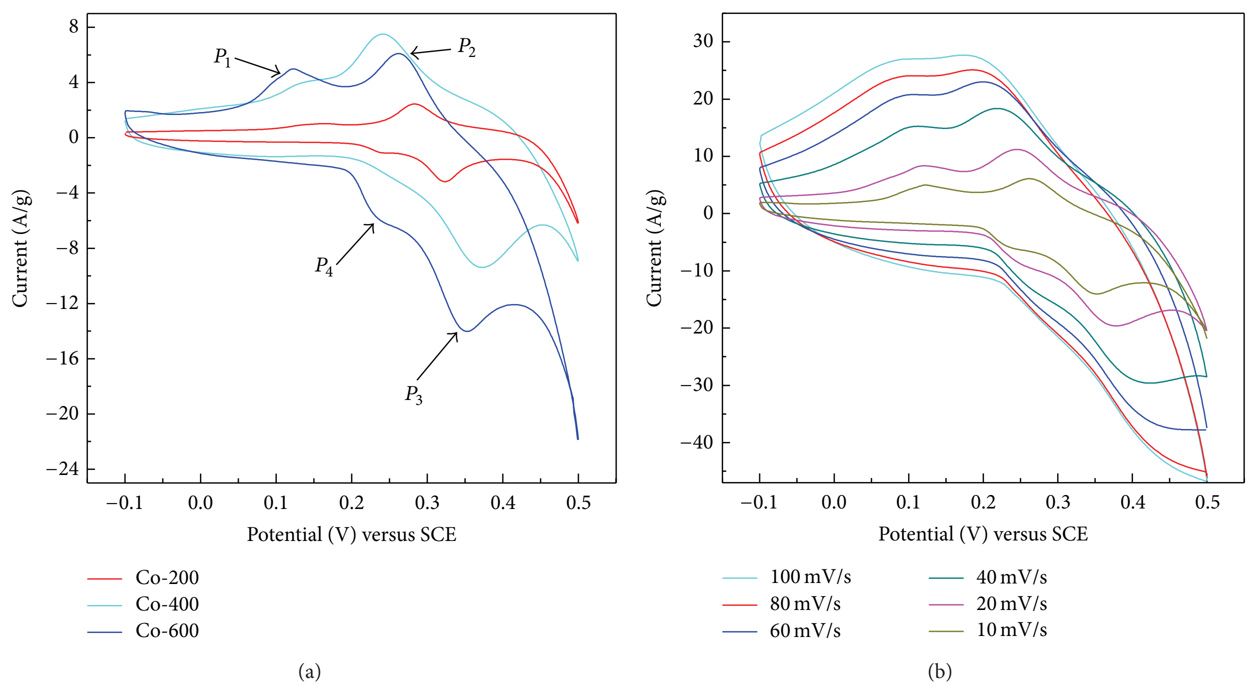

FIGURE 7: (a) Cyclic voltammograms (CV) behavior of samples obtained at different temperatures and (b) cyclic voltammograms (CV) behavior of Co-600 in 6 M KOH electrolyte at various scan rates.

The specific capacitance (C) of the Co-600 can be calculated according to the following equation:

$$C = \frac{1}{mv\left(V_a - V_c\right)} \int_{V_a}^{V_c} I\left(V\right) dV, \quad (7)$$

where C is the specific capacitance (F/g), m is the mass of Co_3O_4 (g), v represents the scan rate (V/s), and $I(V)$ is a current response in accordance with the sweep voltage. V_a denotes the potential (V) when the electrode starts to discharge, and V_c denotes the potential (V) when the electrode ends up discharging. $(V_a - V_c)$ denotes the potential range of CV (V).

In Figure 7(b), based on (7), the specific capacitance of Co-600 is evaluated as 468.18, 326.51, 264.58, 220.26, 198.86, and 171.13 F/g at scan rates of 10, 20, 40, 60, 80, and 100 mV/s, respectively. Such behavior is primarily due to the diffusion of OH^- which becomes slower with the increase of scan rate, and the ions cannot reach the inter surface of Co_3O_4 [37, 38].The capacitance of the synthesized Co_3O_4 is relatively high compared with the results reported of different morphologies of Co_3O_4 [10, 12, 27]. Moreover, with an increase in scan rate, the cathodic and anodic peaks shift to lower and higher potentials, respectively, and the CV curve characteristic shape has not changed significantly, demonstrating that the Co_3O_4 has an outstanding capability and the electrolyte ions have a fast diffusion [39]. We also calculate the electrochemical utilization from $z = C \times \Delta V \times M/F$ [27], where C is the test specific capacitance (F/g), ΔV is the potential range (0.6 V in this study), M is the molecular weight of Co_3O_4 (240.8 g/mol), and F is the Faradic constant (96,486 C/mol). The value of z is 1 if all of the electroactive sites are involved in the Faradic reactions. The z value is 0.701 at a scan rate of 10 mV/s, confirming that the sample prepared shows a high ratio contribution of the electroactive sites.

To acquire more information concerning the capability, electrochemical impedance spectroscopy is employed to show the Nyquist plots for the Co_3O_4 electrode using a sinusoidal signal of 5 mV over the frequency range of 0.01 Hz to 10^5 Hz. The Nyquist plots are given in Figure 8. As is known, the internal resistance of Co_3O_4 electrode in an open circuit can be judged from the point of intersection of the high frequency part at the real axis of the plots [40]. The internal resistance is less than 1.3 Ω, which includes the following terms: the ionic resistance of electrolyte, the intrinsic resistance of the active material, and the contact

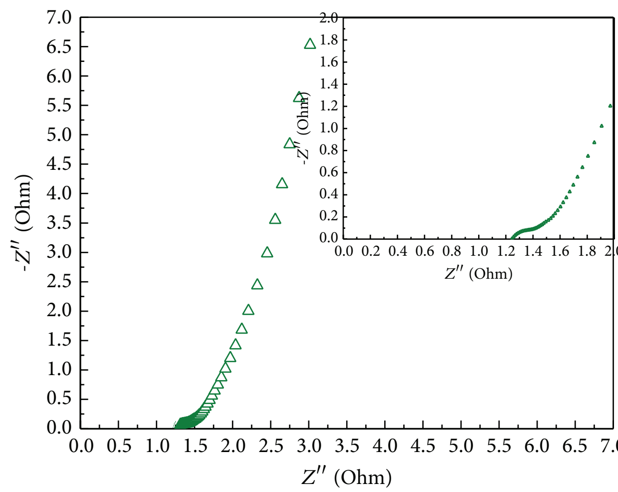

FIGURE 8: Impedance plot of Co-600 electrode.

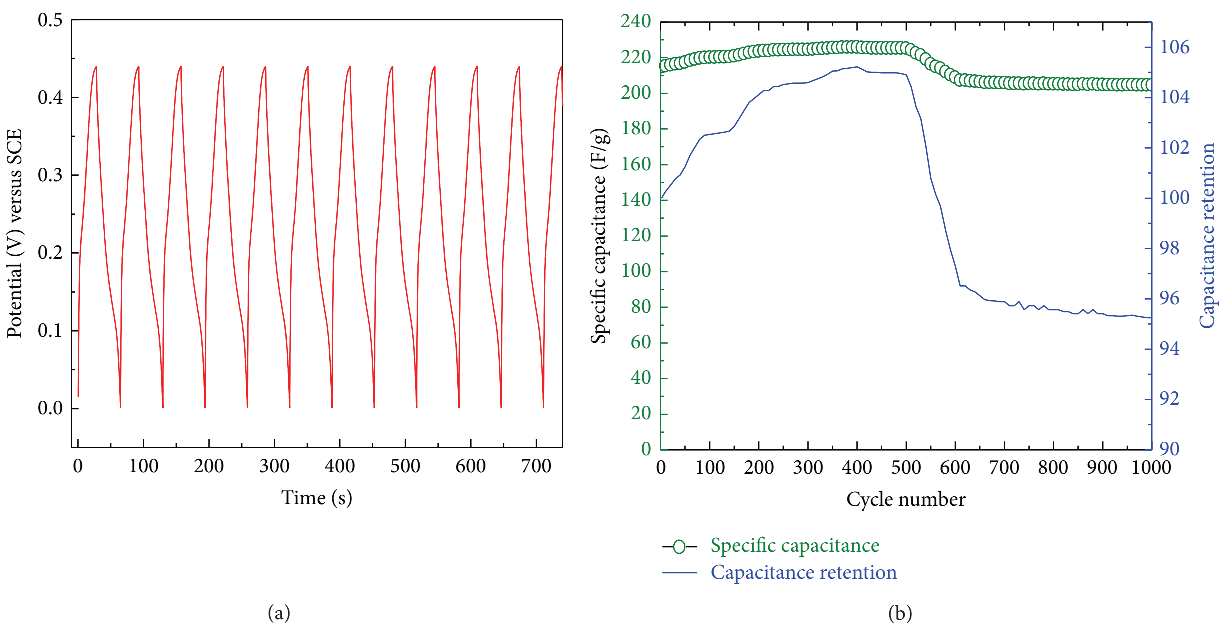

FIGURE 9: (a) Charge-discharge curves and (b) cycle life and capacity retention of the Co-600 at the current density of 3 A/g in 6 M KOH.

resistance at the electrode/current collector interface [41]. Besides, in the up-right corner of Figure 8, a depressed semicircle can be discovered clearly in the high-to-medium frequency region, which is related to Faradic reactions and its diameter represents the interfacial charge transfer resistance at the electrode/electrolyte interface [42], and the value of the charge transfer resistance of the electrode is only ~0.15 Ω. Normally, in the low frequency range, the straight sloping line represents the electrolyte diffusion process and the diffusion of OH^- ion in host materials, and a higher slope of the impedance represents a lower diffusive resistance in the electrode by the shortened diffusion path of OH^- ion [43, 44]. The impedance plot observed in Figure 8 shows a sloppy line of diffusion process in a solid electrode, indicating an excellent capacitive behavior of Co-600 material. All these findings mentioned above demonstrate that the Co_3O_4 prepared have a good frequency response and a fast ionic motion with low diffusive resistance in solid electrode for electrochemical capacitor.

Cyclability of the Co_3O_4 materials as electrodes in electrolyte is one of the important qualities for practical applications. As shown in Figure 9, the Co-600 prepared is charged-discharged at the current density of 3 A/g for 1000 cycles. Figure 9(a) depicts a chronopotentiogram including the initial 11 cycles of the Co_3O_4 electrode in 6 M KOH solution at 3 A/g, from which it can be seen that the charge-discharge process of the electrode is reversible and the charge-discharge curve is asymmetric. The specific capacitance of the electrode can be calculated by using $C = It/\Delta Vm$, in which I is the discharge current, t is the discharge time, ΔV is the potential range during discharge, and m is the mass of active material in the electrode. According to the equation above, the specific capacitance variation of Co_3O_4 samples and the capacitance retention are shown in Figure 9(b). During the first 300 cycles, the specific capacitance increased from 213.33 to 222.93 F/g, which is due to the activation process of the Co_3O_4 electroactive material [12]. Thereafter, the specific capacitance of the Co_3O_4 declines with the increasing cycle number. With cycle up to 1000 times, the supercapacitor still remains 95.2%, suggesting that the Co_3O_4 prepared has an excellent stability for practical application.

4. Conclusions

In summary, Co_3O_4 nanoparticles were successfully prepared by a novel, facile, and environmental carbon-assisted method using degreasing cotton and were furthermore applied as electrodes of supercapacitor. It also confirmed that the additive degreasing cotton played an indispensable role in synthesizing Co_3O_4 with high specific areas. Importantly, the carbon-assisted method using degreasing cotton can be easily extended to prepare other systems concerning metal oxide, such as Fe_3O_4. Electrochemical results indicated that the as-prepared Co_3O_4 can deliver a specific capacitance of 468.18 F/g at a scan rate of 10 mV/s, and the charge transfer resistance of the electrode was only ~0.15 Ω. Particularly, there was only 4.8% decay of the specific capacitance at a current density of 3 A/g upon 1000 cycles. These results showed that the Co_3O_4 we prepared had a promising potential for practical application.

Conflict of Interests

The authors declare that there is no conflict of interests regarding the publishing of this paper.

Acknowledgment

This project was supported by the National Natural Science Foundation of China (no. 91123616 and no. 51105345).

References

[1] J. R. Miller, "Electrochemical capacitor thermal management issues at high-rate cycling," *Electrochimica Acta*, vol. 52, no. 4, pp. 1703–1708, 2006.

[2] Y. Y. Liang, S. J. Bao, and H. L. Li, "Nanocrystalline nickel cobalt hydroxides/ultrastable Y zeolite composite for electrochemical capacitors," *Journal of Solid State Electrochemistry*, vol. 11, no. 5, pp. 571–576, 2007.

[3] Y. S. Chen and C. C. Hu, "Capacitive characteristics of binary manganese-nickel oxides prepared by anodic deposition," *Electrochemical and Solid-State Letters*, vol. 6, no. 10, pp. A210–A213, 2003.

[4] T. A. Centeno and F. Stoeckli, "The role of textural characteristics and oxygen-containing surface groups in the supercapacitor performances of activated carbons," *Electrochimica Acta*, vol. 52, no. 2, pp. 560–566, 2006.

[5] F. C. Wu, R. L. Tseng, C. C. Hu, and C. C. Wang, "Physical and electrochemical characterization of activated carbons prepared from firwoods for supercapacitors," *Journal of Power Sources*, vol. 138, no. 1-2, pp. 351–359, 2004.

[6] V. Subramanian, S. C. Hall, P. H. Smith, and B. Rambabu, "Mesoporous anhydrous RuO_2 as a supercapacitor electrode material," *Solid State Ionics*, vol. 175, no. 1–4, pp. 511–515, 2004.

[7] C. C. Hu, K. H. Chang, M. C. Lin, and Y. T. Wu, "Design and tailoring of the nanotubular arrayed architecture of hydrous RuO_2 for next generation supercapacitors," *Nano Letters*, vol. 6, no. 12, pp. 2690–2695, 2006.

[8] M. Mastragostino, C. Arbizzani, and F. Soavi, "Conducting polymers as electrode materials in supercapacitors," *Solid State Ionics*, vol. 148, no. 3-4, pp. 493–498, 2002.

[9] P. Soudan, H. A. Ho, L. Breau, and D. Belanger, "Chemical synthesis and electrochemical properties of poly(cyano-substituted-diheteroareneethylene) as conducting polymers for electrochemical supercapacitors," *Journal of the Electrochemical Society*, vol. 148, no. 7, pp. A775–A782, 2001.

[10] M. J. Deng, F. L. Huang, I. W. Sun, W. T. Tsai, and J. K. Chang, "An entirelyelectrochemical preparation of a nano-structured cobalt oxide electrode with superior redox activity," *Nanotechnology*, vol. 20, no. 17, Article ID 175602, 2009.

[11] N. Yan, L. Hu, Y. Li et al., "Co_3O_4 nanocages for high-performance anode material in lithium-ion batteries," *Journal of Physical Chemistry C*, vol. 116, no. 12, pp. 7227–7235, 2012.

[12] B. Y. Kim, I. B. Shim, Z. O. Araci et al., "Synthesis and colloidal polymerization of ferromagnetic Au-Co nanoparticles into Au-Co_3O_4 nanowires," *Journal of the American Chemical Society*, vol. 132, no. 10, pp. 3234–3235, 2010.

[13] X. Wang, L. Yu, X. L. Wu et al., "Synthesis of single-crystalline Co_3O_4 octahedral cages with tunable surface aperture and their lithium storage properties," *Journal of Physical Chemistry C*, vol. 113, no. 35, pp. 15553–15558, 2009.

[14] H. Du, L. Jiao, Q. Wang et al., "Facile carbonaceous microsphere templated synthesis of Co_3O_4 hollow spheres and their electrochemical performance in supercapacitors," *Nano Research*, vol. 6, no. 2, pp. 87–98, 2013.

[15] J. Liu, J. Jiang, C. Cheng et al., "Co_3O_4 nanowire@MnO_2 ultrathin nanosheet core/shell arrays: a new class of high-performance pseudocapacitive materials," *Advanced Materials*, vol. 23, no. 18, pp. 2076–2081, 2011.

[16] P. Zhang, G. X. Hu, S. J. Bao et al., "One step microwave synthesis and magnetic properties of Co_3O_4 octahedrons," *Materials Letters*, vol. 83, pp. 195–197, 2012.

[17] G. Gundiah, A. Govindaraj, and C. N. R. Rao, "Nanowires, nanobelts and related nanostructures of Ga_2O_3," *Chemical Physics Letters*, vol. 351, no. 3-4, pp. 189–194, 2002.

[18] J. Y. Lao, J. G. Wen, and Z. F. Ren, "Hierarchical ZnO nanostructures," *Nano Letters*, vol. 2, no. 11, pp. 1287–1291, 2002.

[19] Y. C. Zhu, Y. Bando, D. F. Xue, and D. Golberg, "Nanocable-aligned ZnS tetrapod nanocrystals," *Journal of the American Chemical Society*, vol. 125, no. 52, pp. 16196–16197, 2003.

[20] J. Jie, G. Wang, X. Han et al., "Growth and properties of well-aligned ZnO hexagonal cones prepared by carbonthermal reaction," *Journal of Crystal Growth*, vol. 267, no. 1-2, pp. 223–230, 2004.

[21] F. Wang, G. Q. Jin, and X. Y. Guo, "Formation mechanism of Si_3N_4 nanowires via carbothermal reduction of carbonaceous silica xerogels," *Journal of Physical Chemistry B*, vol. 110, no. 30, pp. 14546–14549, 2006.

[22] H. Zhao, M. Lei, X. Yang, J. Jian, and X. Chen, "Route to GaN and VN assisted by carbothermal reduction process," *Journal of the American Chemical Society*, vol. 127, no. 45, pp. 15722–15723, 2005.

[23] Q. Zhang, J. Li, X. Chou et al., "Synthesis of superparamagnetic iron oxide nanoparticles in carbon reduction method," *Micro & Nano Letters*, vol. 8, no. 10, pp. 598–601, 2013.

[24] H. Li, G. T. Fei, M. Fang et al., "Synthesis of urchin-like Co_3O_4 hierarchical micro/nanostructures and their photocatalytic activity," *Applied Surface Science*, vol. 257, no. 15, pp. 6527–6530, 2011.

[25] Y. Liu, G. Zhu, B. Ge et al., "Concave Co_3O_4 octahedral mesocrystal: polymer-mediated synthesis and sensing properties," *CrystEngComm*, vol. 14, no. 19, pp. 6264–6270, 2012.

[26] S. Farhadi, K. Pourzare, and S. Sadeghinejad, "Simple preparation of ferromagnetic Co_3O_4 nanoparticles by thermal dissociation of the $[Co(NH_3)_6](NO_3)_2$ complex at low temperature," *Journal of Nanostructure in Chemistry*, vol. 3, no. 1, pp. 1–7, 2013.

[27] M. Aghazadeh, "Electrochemical preparation and properties of nanostructured Co_3O_4 as supercapacitor material," *Journal of Applied Electrochemistry*, vol. 42, no. 2, pp. 89–94, 2012.

[28] T. He, D. Chen, X. Jiao, Y. Xu, and Y. Gu, "Surfactant-assisted solvothermal synthesis of Co_3O_4 hollow spheres with oriented-aggregation nanostructures and tunable particle size," *Langmuir*, vol. 20, no. 19, pp. 8404–8408, 2004.

[29] N. Zotov, K. Petrov, and M. Dimitrova-Pankova, "Infrared spectra of Cu(II)-Co(II) mixed hydroxide nitrates," *Journal of Physics and Chemistry of Solids*, vol. 51, no. 10, pp. 1199–1205, 1990.

[30] J. Xu, P. Gao, and T. S. Zhao, "Non-precious Co_3O_4 nano-rod electrocatalyst for oxygen reduction reaction in anion-exchange membrane fuel cells," *Energy and Environmental Science*, vol. 5, no. 1, pp. 533–539, 2012.

[31] G. Kwak, J. Hwang, J. Y. Cheon et al., "Preparation method of Co_3O_4 nanoparticles using ordered mesoporous carbons as a template and their application for fischer-tropsch synthesis," *The Journal of Physical Chemistry C*, vol. 117, no. 14, pp. 1773–1779, 2013.

[32] F. Zhang, L. Hao, L. Zhang, and X. Zhang, "Solid-state thermolysis preparation of Co_3O_4 nano/micro superstructures from metal-organic framework for supercapacitors," *International Journal of Electrochemical Science*, vol. 6, no. 7, pp. 2943–2954, 2011.

[33] X. Wang, L. Yu, P. Hu, and F. Yuan, "Synthesis of single-crystalline hollow octahedral NiO," *Crystal Growth and Design*, vol. 7, no. 12, pp. 2415–2418, 2007.

[34] T. Zhu, Y. Liu, Z. Hu, C. Wang, and Z. Wen, "Preparation and characterization of mesoporous Co_3O_4 electrode material," *Journal of Materials Science: Materials in Electronics*, vol. 22, no. 11, pp. 1649–1655, 2011.

[35] J. Chen, K. Huang, and S. Liu, "Insoluble metal hexacyanoferrates as supercapacitor electrodes," *Electrochemistry Communications*, vol. 10, no. 12, pp. 1851–1855, 2008.

[36] C. Barbero, G. A. Planes, and M. C. Miras, "Redox coupled ion exchange in cobalt oxide films," *Electrochemistry Communications*, vol. 3, no. 3, pp. 113–116, 2001.

[37] C. Xu, B. Li, H. Du, F. Kang, and Y. Zeng, "Electrochemical properties of nanosized hydrous manganese dioxide synthesized by a self-reacting microemulsion method," *Journal of Power Sources*, vol. 180, no. 1, pp. 664–670, 2008.

[38] V. Subramanian, H. Zhu, R. Vajtai, P. M. Ajayan, and B. Wei, "Hydrothermal synthesis and pseudocapacitance properties of MnO_2 nanostructures," *Journal of Physical Chemistry B*, vol. 109, no. 43, pp. 20207–20214, 2005.

[39] H. W. Wang, Z. A. Hu, Y. Q. Chang et al., "Preparation of reduced graphene oxide/cobalt oxide composites and their enhanced capacitive behaviors by homogeneous incorporation of reduced graphene oxide sheets in cobalt oxide matrix," *Materials Chemistry and Physics*, vol. 130, no. 1-2, pp. 672–679, 2011.

[40] V. Khomenko, E. Raymundo-Piñero, and F. Béguin, "Optimisation of an asymmetric manganese oxide/activated carbon capacitor working at 2V in aqueous medium," *Journal of Power Sources*, vol. 153, no. 1, pp. 183–190, 2006.

[41] L. Cui, J. Li, and X. G. Zhang, "Preparation and properties of Co_3O_4 nanorods as supercapacitor material," *Journal of Applied Electrochemistry*, vol. 39, no. 10, pp. 1871–1876, 2009.

[42] L. Xie, K. Li, G. Sun et al., "Preparation and electrochemical performance of the layered cobalt oxide (Co_3O_4) as supercapacitor electrode material," *Journal of Solid State Electrochemistry*, vol. 17, no. 1, pp. 55–61, 2013.

[43] Y. Li, K. Huang, S. Liu, Z. Yao, and S. Zhuang, "Meso-macroporous Co_3O_4 electrode prepared by polystyrene spheres and carbowax templates for supercapacitors," *Journal of Solid State Electrochemistry*, vol. 15, no. 3, pp. 587–592, 2011.

[44] M. S. Wu and H. H. Hsieh, "Nickel oxide/hydroxide nanoplatelets synthesized by chemical precipitation for electrochemical capacitors," *Electrochimica Acta*, vol. 53, no. 8, pp. 3427–3435, 2008.